Nano Research 2013, 6(4): 243–252
DOI 10.1007/s12274-013-0300-3
Research Article

ISSN 1998-0124
CN 11-5974/O4

Kinetics-controlled growth of aligned mesocrystalline SnO_2 nanorod arrays for lithium-ion batteries with superior rate performance

Shuai Chen, Miao Wang, Jianfeng Ye, Jinguang Cai, Yurong Ma, Henghui Zhou (✉), and Limin Qi (✉)

Beijing National Laboratory for Molecular Sciences, State Key Laboratory for Structural Chemistry of Unstable and Stable Species, College of Chemistry, Peking University, Beijing 100871, China

Received: 8 January 2013
Revised: 30 January 2013
Accepted: 17 February 2013

KEYWORDS
tin dioxide,
nanostructures,
mesocrystals,
hierarchical structures,
lithium-ion batteries

ABSTRACT

A general method for facile kinetics-controlled growth of aligned arrays of mesocrystalline SnO_2 nanorods on arbitrary substrates has been developed by adjusting supersaturation in a unique ternary solvent system comprising acetic acid, ethanol, and water. The hydrolysis processes of Sn(IV) as well as the nucleation and growth of SnO_2 crystals were carefully controlled in the mixed solvents, leading to an exclusively heterogeneous nucleation on a substrate and the subsequent growth into mesocrystalline nanorod arrays. In particular, aligned arrays of hierarchically structured, [001]-oriented mesocrystalline SnO_2 nanorods with four {110} lateral facets can be readily grown on Ti foil, as well as many other inert substrates such as fluoride-doped tin oxide (FTO), Si, graphite, and polytetrafluoroethylene (Teflon). Due to the unique combination of the mesocrystalline structure and the one-dimensional nanoarray structure, the obtained mesocrystalline SnO_2 nanorod arrays grown on metallic Ti substrate exhibited an excellent rate performance with a high initial Coulombic efficiency of 65.6% and a reversible capacity of 720 mA·h/g at a charge/discharge rate of 10 C (namely, 7,820 mA/g) when used as an anode material for lithium-ion batteries.

1 Introduction

Lithium-ion batteries (LIBs) have been considered as the most promising energy storage technology for a wide variety of applications including portable electronics, electric vehicles, and stationary energy storage systems for solar and wind energy [1, 2]. Significant efforts have been devoted to the development of novel nanostructured electrode materials to meet the requirements for high energy density and high power density [3–10]. Owing to its high theoretical capacity of ~782 mA·h/g, low working potential of ~0.6 V (vs. Li^+/Li), and easy modification of nanostructures, SnO_2 has been regarded as one of the most

Address correspondence to Henghui Zhou, hhzhou@pku.edu.cn; Limin Qi, liminqi@pku.edu.cn

promising candidates for future green anode materials in LIBs [11–15]. However, its practical application as anode materials is significantly limited by the large irreversible capacity loss in the first cycle and the poor cycling performance, which are mainly caused by the large volume change (~250%) during lithium insertion/extraction processes [11–13, 16]. In this regard, a variety of SnO_2 nanostructures, such as nanowires [14], nanosheets [15], hollow structures [17–20], and porous structures [21, 22], as well as SnO_2-carbon nanotubes [23] and SnO_2–graphene nanocomposites [24–26] have been developed to improve the lithium storage performance of SnO_2 anode materials. Nevertheless, it remains a challenge to reduce the irreversible capacity loss in the first cycle and increase the reversible capacity at high rate through fabricating hierarchical SnO_2 architectures with deliberate high-order nanostructures.

In recent years, it has been shown that one-dimensional (1D) oxide nanostructure arrays directly grown on conductive metal substrates may provide desirable LIB anodes with remarkable advantages including enhanced rate capability [12, 27, 28]. While chemical vapor deposition (CVD) [29] and template-assisted synthesis [30, 31] have been employed for the controlled synthesis of SnO_2 nanorod, nanowire, and nanotube arrays, hydrothermal growth without templates [28, 32–34] has turned out to be very effective in the facile, large-scale fabrication of SnO_2 nanorod/nanowire arrays on specific substrates. However, there are few reports of the direct growth of aligned arrays of 1D SnO_2 nanostructures with complex superstructures or hierarchical architectures on conductive substrates, probably owing to the difficulty in the accurate control of the fast hydrolysis processes of tin-containing precursors. It is noteworthy that as hierarchical assemblies of crystallographically oriented nanocrystals, mesocrystals are receiving increasing attention due to their properties such as high crystallinity, high porosity, and oriented subunit alignment [35–38]. In particular, mesocrystals of both anatase [39] and rutile [40] TiO_2 exhibit enhanced lithium insertion behavior including increased rate capability due to the interconnected nanoscale subunits and interspaces between them. It is expected that a rational combination of a nanorod array structure and a mesocrystalline structure for SnO_2 would lead to LIB anodes with improved performance.

Herein, we report a facile kinetics-controlled growth of aligned arrays of mesocrystalline SnO_2 nanorods on arbitrary substrates in a unique ternary solvent system comprising acetic acid, ethanol, and water. The reaction kinetics was controlled by carefully adjusting the supersaturation in the mixed solvents, leading to a heterogeneous nucleation on the substrate and the subsequent growth into mesocrystalline SnO_2 nanorod arrays. To the best of our knowledge, this is the first synthesis of mesocrystalline structures for SnO_2. The obtained mesocrystalline SnO_2 nanorod arrays grown on metallic Ti substrate exhibited a superior rate performance with a high initial Coulombic efficiency (65.6%) and a reversible capacity of 720 mA·h/g at a charge/discharge rate of 10 C (1 C = 782 mA/g) when used as an anode material for LIBs.

2 Experimental

2.1 Synthesis of SnO_2 nanorod arrays

Ti foils (~0.25 mm in thickness, 99.7%, Sigma–Aldrich) were cleaned by sonication in acetone, ethanol, deionized (DI) water, and finally dried in air. SnO_2 nanorod arrays were solvothermally synthesized in a ternary solvent system comprising acetic acid, ethanol, and water using $SnCl_4$ as the Sn source and NaBr as the additive. In a typical synthesis, NaBr (0.3 mmol) was dissolved in 1 mL of DI water, and $SnCl_4{\cdot}5H_2O$ (0.1 mmol) was dissolved in 6 mL of glacial acetic acid. Then, these two clear solutions were mixed with 1 mL of ethanol under continuous stirring, resulting in a pale yellow solution. The mixed solution was transferred into a 25 mL Teflon-lined stainless steel autoclave where a circular Ti foil ~1 cm in diameter or a square Ti foil ~1 cm in edge length was placed, which was then heated at 200 ℃ for 24 h. After the autoclave was cooled to room temperature, the substrate was cleaned with DI water, sonicated in ethanol, and then dried in air. The loading density of SnO_2 on Ti foil was estimated to be around 0.55 mg/cm^2 by measuring the weight of the bare Ti foil and that of the Ti foil covered by SnO_2 nanorod arrays. Similarly, small pieces (~1 cm^2 square) of fluoride-doped tin oxide (FTO) glass, Si

slices, graphite slices, and polytetrafluoroethylene (Teflon) slices were used as substrates for the growth of SnO_2 nanorod arrays with comparable loading densities.

2.2 Characterization

The products were characterized by scanning electron microscopy (SEM, Hitachi S4800, 5 kV), X-ray diffraction (XRD, Rigaku DMAX-2000, Cu Kα radiation), transmission electron microscopy (TEM, FEI Tecnai T20, 200 kV), and high-resolution TEM (HRTEM, FEI Tecnai F30, 300 kV). The IR analysis was conducted on a Fourier transform IR spectroscopy (FTIR, Nicolet Magna-IR 750) and a Thermo Scientific Nicolet iN10MX Infrared Imaging Microscope (tFTIRM).

2.3 Electrochemical measurements

A circular Ti foil with a diameter of ~1 cm was used as the substrate for the growth of SnO_2 nanorod arrays, which were calcined at 450 ℃ for 30 min to remove organic species and dried under vacuum at 120 ℃ overnight before electrochemical measurements. The weight of SnO_2 was calculated by subtracting the weight of the bare Ti foil from that of the Ti foil with SnO_2 nanorod arrays. The Ti foil with SnO_2 nanorod arrays grown on one face was directly used as an anode in a 2032 coin cell, which was assembled in an argon-filled glovebox. The bare face of the Ti foil was located close to the outside shell of the cell. Li foil was used as the counter electrode, 1 M $LiClO_4$ in propylene carbonate (PC) and dimethyl carbonate (1:1 by volume) was used as the electrolyte, and Celgard 2400 was used as the separator. The electrochemical performances were tested by using a LAND CT2001A battery test system at room temperature (25 ℃). The coin cells were discharged and charged between 2.5 V and 0.05 V at a constant current (1 C rate taken to be 782 mA/g).

3 Results and discussion

3.1 Morphology and structure

Mesocrystalline SnO_2 nanorod arrays were readily grown on Ti foil by a solvothermal process in a ternary solvent system comprising acetic acid (HAc), ethanol, and water using $SnCl_4$ as the Sn source and NaBr as the additive. The color of the Ti foil changed from silvery white to orange after the growth of a uniform SnO_2 thin film owing to the thin film interference (Fig. S1 in the Electronic Supplementary Material (ESM)). Figure 1(a) shows a typical low-magnification SEM image of the SnO_2 products on Ti foil after solvothermal reaction at 200 ℃ for 24 h, which suggests the formation of uniform nanorod arrays on a large area (an enlarged SEM image is shown in Fig. S2 in the ESM). The high-magnification SEM image shown in Fig. 1(b) suggests that each nanorod has a square cross section and the square nanorods have an average edge length of ~80 nm. Moreover, it shows that all the nanorods exhibit rough top surfaces, indicating that each square nanorod consists of a bundle of primary nanorods. As shown in Fig. 1(c), the nanorod arrays have a length of ~750 nm and the square nanorods are actually made of bundles of primary nanorods around 10 nm in width (an enlarged SEM image is shown in Fig. S2 in the ESM). The XRD pattern of the SnO_2 nanorod arrays is shown in Fig. 1(d), which suggests the formation of pure SnO_2 crystals with a tetragonal rutile phase (JCPDS No. 41-1445) on the Ti substrate. The significantly increase in the intensity of the (002) peak compared with the standard pattern indicates that these nearly vertical SnO_2 nanorods are preferentially grown along the [001] direction.

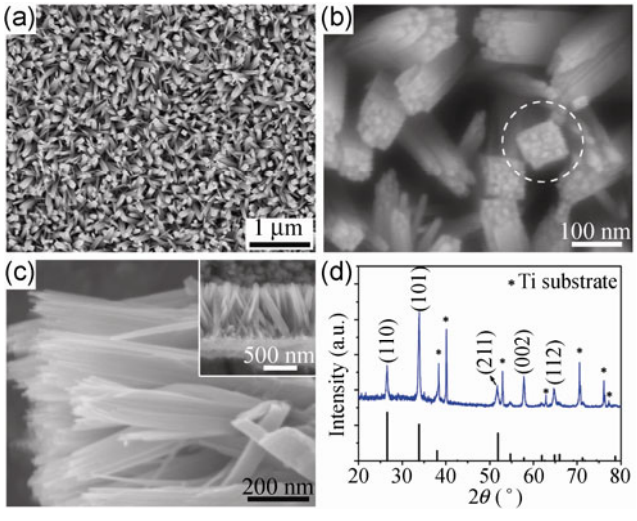

Figure 1 SEM images (a)–(c) and XRD pattern (d) of mesocrystalline SnO_2 nanorod arrays grown on Ti foil. The inset in (c) shows the low-magnification cross-section image.

The mesocrystalline structure of the SnO_2 nanorods with a square cross section was revealed by TEM observations shown in Fig. 2. The TEM image of a typical SnO_2 nanorod suggests that the nanorod consists of a bundle of primary nanorod subunits (Fig. 2(a)). The corresponding selected-area electron diffraction (SAED) pattern exhibits the single-crystalline diffraction features of rutile SnO_2, indicating that each nanorod is a [001]-oriented, single-crystal-like SnO_2 mesocrystal consisting of a bundle of primary nanorods. It also indicates that the SnO_2 nanorod with a square cross section has four side surfaces enclosed by {110} planes since the tetragonal nanorod tends to lie on its flat lateral faces. A high-magnification image of the top end of the SnO_2 nanorod clearly shows the presence of parallel primary nanorods ~10 nm in width with some interspaces between them (Fig. 2(b)). The middle part of the SnO_2 nanorod shows some parallel stripes arising from the superposition of several layers of primary nanorods aligned in parallel (Fig. 2(c)), confirming that the whole nanorod is a SnO_2 mesocrystal consisting of a bundle of parallel primary nanorods with interspaces. The HRTEM image shown in Fig. 2(d) shows that the parallel primary nanorods exhibit clear lattice fringes with spacings of 0.32 nm and 0.34 nm, which correspond to the (001) and (110) planes of rutile SnO_2, respectively. It demonstrates that each primary nanorod is a [001]-oriented SnO_2 single crystal and the parallel alignment of the primary nanorods leads to a novel tetragonal nanorod mesocrystal with four {110} lateral facets. It may be noted that aligned arrays of [001]-oriented, single-crystalline SnO_2 nanorods with four side surfaces enclosed by the {110} planes have previously been grown hydrothermally on Fe–Co–Ni alloy foil in an aqueous alkaline solution as a result of the crystallographic habit of SnO_2 [28]. In the current situation, the unique growth conditions in the acidic ternary solvent system resulted in aligned arrays of the novel hierarchically structured, [001]-oriented mesocrystalline SnO_2 nanorods with four {110} lateral facets grown on Ti foil.

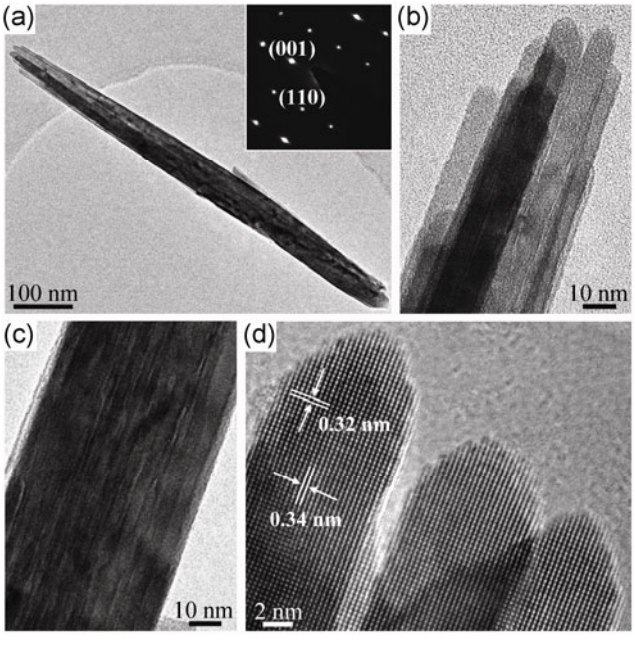

Figure 2 TEM (a)–(c) and HRTEM (d) images of mesocrystalline SnO_2 nanorods. The inset in (a) is the SAED pattern of the whole nanorod shown in Panel (a). Panels (b) and (c) are high-magnification images of the top end and middle part of the nanorod in Panel (a), respectively.

3.2 Effects of solvent

It was found that appropriate mixing ratios of the three solvents in the ternary solvent system are essential to the formation of mesocrystalline SnO_2 nanorod arrays on Ti foil. An optimal synthesis condition for the mesocrystalline SnO_2 nanorod arrays was a ternary solvent system comprising 6 mL of acetic acid, 1 mL of ethanol, and 1 mL of water. The hydrolysis of $SnCl_4$ in ternary solvent systems with varying amounts of water, acetic acid, and ethanol were investigated. Figure 3 shows the SnO_2 products obtained with different amounts of water under otherwise identical conditions. When the amount of water was decreased from 1 mL to 0.75 mL, the hydrolysis of $SnCl_4$ was very slow and only small cube-like nanoparticles appeared on the substrate after 24 h of growth (Fig. 3(a)). If the amount of water was increased from 1 mL to 1.5 mL, denser arrays of mesocrystalline SnO_2 nanorods consisting of thicker primary nanorods were grown on the substrate (Figs. 3(b) and 3(c)). When the amount of water was further increased to 2 mL, many micrometer-sized urchin-like particles were produced in the solution rather than grown on the substrate, as shown in Fig. 3(d). These urchin-like particles essentially exhibited a core–shell structure and the shells were composed of radially aligned, [001]-oriented SnO_2 nanorods made of primary nanorod bundles (Figs. 3(e) and 3(f)). This

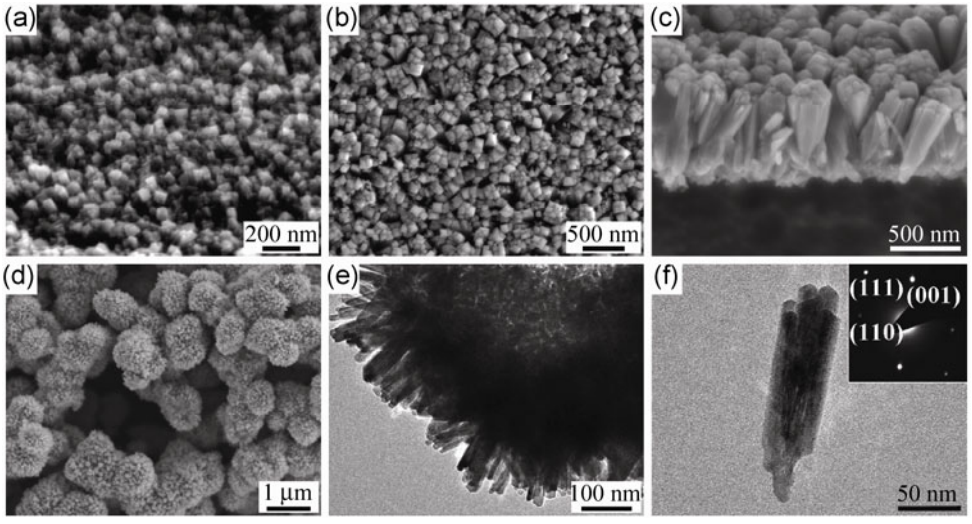

Figure 3 SEM images (a)–(d) and TEM images (e) and (f) of SnO_2 products obtained with different amounts of water: (a) 0.75 mL, (b) and (c) 1.5 mL, (d)–(f) 2 mL. The inset in (f) is the SAED pattern of a bundle of nanorods which has fallen off the urchin-like particles.

result indicates that the hydrolysis process of $SnCl_4$ was accelerated with increasing water content, leading to significant increase in the supersaturation and hence a transition from heterogeneous nucleation on the substrate to homogeneous nucleation in solution. The presence of appropriate contents of HAc and ethanol was also necessary for the formation of well-defined, mesocrystalline SnO_2 nanorod arrays. At a lower HAc content or higher ethanol content, the reaction was accelerated and the mesocrystalline SnO_2 nanorod arrays became denser; in contrast, at a higher HAc content or a lower ethanol content, the reaction was slowed down and SnO_2 nanoparticles were grown on the substrate instead of SnO_2 nanorods (Fig. S3 in the ESM). These results indicate that the formation of mesocrystalline SnO_2 nanorod arrays on the substrate may result from a kinetics-controlled growth under appropriate supersaturation conditions [41].

It is known that carboxylic acids can coordinate with Sn^{4+} ions to form intermediate complexes of Sn(IV), which can be further hydrolyzed into SnO_2 nanocrystals through hydrolysis and esterification in mixed alcohol/acid systems [42]. We propose that the mesocrystalline SnO_2 nanorods proceeded by similar reactions (Eqs. (1–3))

$$SnCl_4 + xCH_3COOH \longrightarrow SnCl_{4-x}(CH_3COO)_x + xCl^- + xH^+ \quad (1)$$

$$SnCl_{4-x}(CH_3COO)_x + H_2O \longrightarrow SnO_2\,(s) + CH_3COOH + Cl^- \quad (2)$$

$$SnCl_{4-x}(CH_3COO)_x + C_2H_5OH \longrightarrow SnO_2\,(s) + CH_3COOC_2H_5 + Cl^- \quad (3)$$

The coordination of CH_3COO^- ions with Sn^{4+} ions will greatly lower the hydrolysis reactivity of Sn^{4+} ions and thus decrease the hydrolysis rate. On the other hand, increasing water content will accelerate the hydrolysis processes. The presence of ethanol may favor the formation of SnO_2 and generation of ethyl acetate via the esterification pathway as shown in Eq. (3), thus accelerating the overall hydrolysis processes. Therefore, appropriate ratios of acetic acid, ethanol, and water result in a suitable rate of hydrolysis of $SnCl_4$ and hence an appropriate supersaturation for heterogeneous nucleation of SnO_2 on the Ti substrate. Meanwhile, ethanol may react directly with acetic acid to form ethyl acetate under the solvothermal conditions. The generation of ethyl acetate was evidenced by an intense odor of ester from reaction solution and the absorption at 1,244 cm^{-1} (C–O stretch of ethyl acetate) in the FTIR spectrum of the solution after reaction (Fig. S4(a) in the ESM). It is noteworthy that the FTIR spectrum of the as-prepared mesocrystalline SnO_2 nanorods indicates the incorporation of a small amount of organic species such as ethyl acetate within the mesocrystalline nanorods (Fig. S4(b) in the ESM),

which could effectively prevent a bundle of subunits from merging into a single-crystalline nanorod. Our preliminary experiments showed that it was difficult to prepare mesocrystalline SnO_2 nanorod arrays in the binary solvent system comprising only acetic acid and water, suggesting that ethanol was indispensable to the formation of the hierarchical mesocrystalline structure. In addition, the presence of a certain concentration of NaBr as additive favored the formation of loosely aligned arrays of mesocrystalline SnO_2 nanorods (Fig. S5 in the ESM), probably as a result of the change in ionic strength, and the coordinating ability of halide ions [33].

3.3 Growth mechanism

The growth process of mesocrystalline SnO_2 nanorod arrays on Ti foil was investigated by examining the products obtained at earlier growth stages, as shown in Fig. 4. At a reaction time of 3 h, many short and thin nanorods showing rough top surfaces were grown on the substrate (Figs. 4(a) and 4(b)), which indicated the heterogeneous nucleation of mesocrystalline nuclei. When the reaction time was extended to 6 h, longer and wider nanorods showing a clear mesocrystalline structure were produced (Figs. 4(c) and 4(d)), which finally evolved into the typical mesocrystalline SnO_2 nanorod arrays shown in Fig. 1 after 24 h of reaction. Accordingly, we proposed a tentative mechanism for the kinetics-controlled growth of mesocrystalline SnO_2 nanorod arrays involving three stages, as shown in Scheme 1. In the acidic ternary solvent system comprising HAc, ethanol, and water with appropriate ratios, the hydrolysis processes of Sn(IV) are carefully controlled and the supersaturation is kept above the critical concentration for the heterogeneous nucleation on the substrate but below the critical concentration for the homogeneous nucleation in solution, resulting in the exclusive nucleation of SnO_2 on the substrate (Stage I). Meanwhile, organic ligands such as HAc and ethyl acetate are adsorbed on the surface of the initial nuclei thus reducing the surface energy and are then wrapped in nucleating crystals, forming initial mesocrystalline nuclei. As the hydrolysis processes progress, the initial SnO_2 nuclei grow in height and width, evolving into well-defined, tetragonal SnO_2 nanorods consisting of a bundle of [001]-oriented

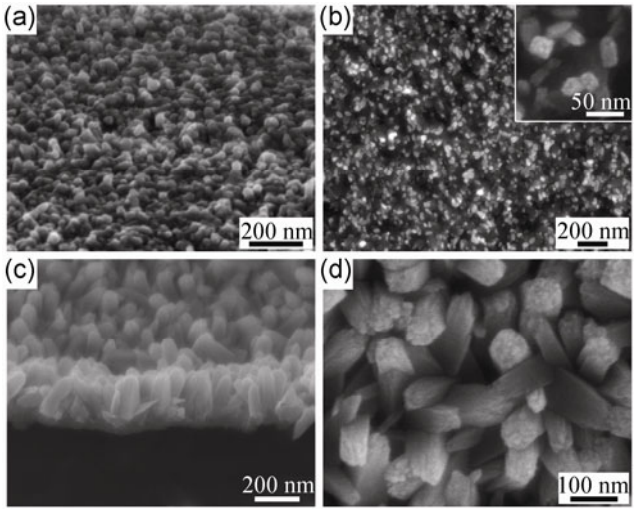

Figure 4 Tilt view (a) and (c); and top view (b) and (d) SEM images of mesocrystalline SnO_2 nanorods grown on Ti foil for different times: (a) and (b) 3 h; (c) and (d) 6 h.

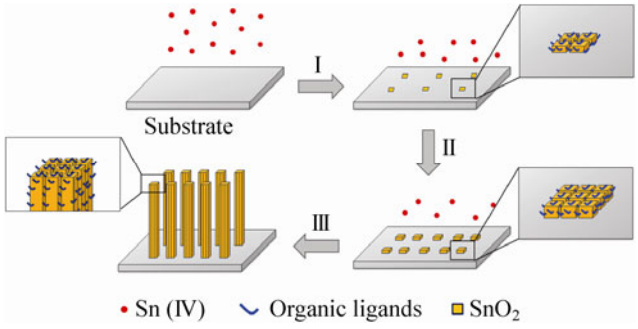

Scheme 1 Schematic illustration of a tentative mechanism for the growth of mesocrystalline SnO_2 nanorod arrays on a substrate.

primary nanorods (Stage II). Then, the [001]-oriented nanorod subunits in the mesocrystalline nuclei grow independently along the [001] direction and finally form mesocrystalline nanorod arrays with organic ligands filled in the interspaces to prevent the fusion of subunits (Stage III). Therefore, the combination of HAc, ethanol, and water plays key roles in the final formation of mesocrystalline SnO_2 nanorod arrays. It is worth noting that such a kinetics-controlled growth process is not limited to the Ti substrate and can be extended to many other solid substrates that are able to withstand the solvothermal conditions. As proof of the generality of the growth on arbitrary inert substrates, similar mesocrystalline SnO_2 nanorod arrays were successfully grown on FTO, Si, graphite, and Teflon in the ternary solvent system comprising HAc, ethanol, and water (Fig. 5). These results indicated that

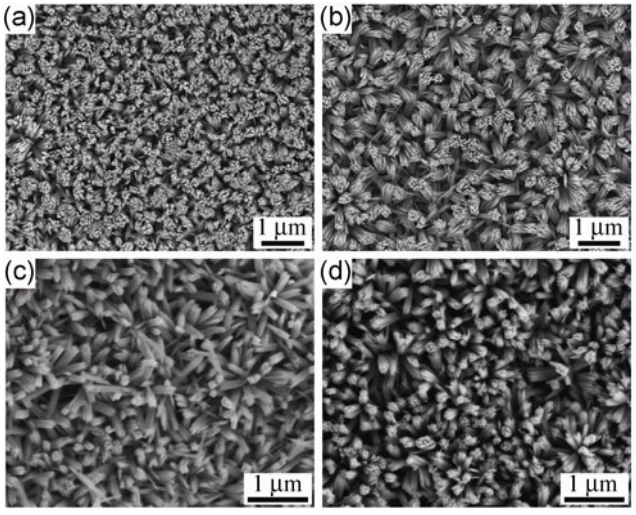

Figure 5 SEM images of mesocrystalline SnO_2 nanorod arrays grown on different substrates: (a) FTO, (b) Si, (c) graphite, (d) Teflon.

the growth process was independent of the substrate, and that the heterogeneous nucleation of mesocrystals can occur on chemically inert substrates like graphite and Teflon. The facile growth of mesocrystalline SnO_2 nanorod arrays on arbitrary substrates may endow SnO_2 nanoarrays with promising potential for applications in various fields including sensing [43], field emission [29], photovoltaics [33, 44], and LIBs [27, 28, 31].

3.4 High rate performance in LIBs

Mesocrystalline SnO_2 nanorod arrays grown on a circular Ti foil ~1 cm in diameter was calcined at 450 °C to remove organic species, and then was directly used as an anode for LIBs to construct a coin cell for electrochemical test. The SnO_2 nanorod arrays retained their mesocrystalline structure and original morphology after removal of the organic species by calcination (Fig. S6 in the ESM). Figure 6(a) shows the charge/discharge voltage profiles at different current rates (1 C = 782 mA/g). Surprisingly, high Coulombic efficiency (CE) values of 67.9%, 71.9%, and 65.6% were observed in the first cycle at charge/discharge rates of 0.2 C, 5 C, and 10 C, respectively, which were higher than those of most SnO_2 nanostructures (normally lower than 50%) and surpassed the high value of 61% at a current rate of 200 mA/g recently reported for SnO_2 nanotube arrays grown on a Ti substrate [31]. A higher initial CE indicates a smaller irreversible capacity loss in the first cycle and a higher reversible capacity. The cycle performances of the mesocrystalline SnO_2 nanorod arrays at different current rates are shown in Fig. 6(b), which shows that the reversible discharge capacity at 0.2 C was 980 mA·h/g, and 89% and 74% of the initial value were retained as the current rate was increased to 5 C and 10 C, respectively. At a current rate as high as 10 C (i.e., 7,820 mA/g), these nanorod arrays exhibited an excellent reversible discharge capacity of 720 mA·h/g and retained 590 mA·h/g after 20 cycles (Fig. 6(c)), values which are much higher than the reversible capacities reported for the SnO_2 nanowire arrays grown on metallic substrates at comparable charge/discharge rates, e.g., 440 mA·h/g at 10 C for the sample obtained by the vapor–liquid–solid (VLS) method [27] and 350 mA·h/g at 5 C for the sample obtained by a hydrothermal method [28]. Moreover, the CE remained over 96% after the third cycle at the high current density of 10 C. Such a superior rate performance is of great importance for fabricating LIBs with improved energy density and power density for future high-power applications. However, it may be pointed out that the measured discharge capacity at 10 C started to drop quickly after 20 cycles and it became as low as ~15 mA·h/g after 50 cycles owing to the significant peeling of the SnO_2 nanorod arrays from the Ti foil during cycling at the high charge/discharge rate. The cycling performance of these electrodes could be improved by surface modification or carbon-coating [45] to meet the requirements of practical applications in the future.

The superior rate performance of the mesocrystalline SnO_2 nanorod arrays on Ti foil as an anode for LIBs could be attributed to the combination of the 1D nanoarray structure and the unique mesocrystalline structure, as shown in Fig. 6(d). On the one hand, the mesocrystalline SnO_2 nanorod arrays maintain all the advantageous features of 1D nanostructure arrays on conductive metal substrates [12], namely, short diffusion length and facile strain relaxation owing to the 1D nanostructure, the protective structural buffer against volume change offered by the interval space between neighboring nanorods, and fast electron transport owing to the robust adhesion of arrayed

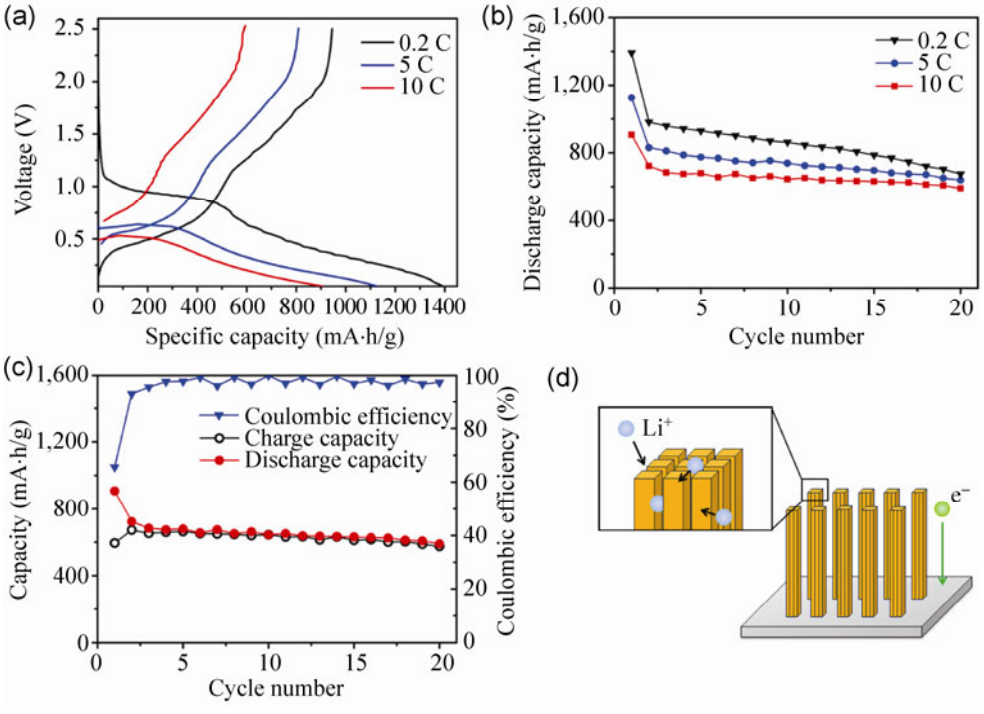

Figure 6 Voltage profiles (a) and cycling performance (b) of mesocrystalline SnO_2 nanorod arrays at different current rates. (c) Charge/discharge capacity and Coulombic efficiency of mesocrystalline SnO_2 nanorod arrays cycled at 10 C. (d) Schematic illustration of mesocrystalline SnO_2 nanorod arrays during the electrochemical process.

nanorods to the conductive substrate and their large contact area with the electrolyte. On the other hand, the hierarchically ordered mesocrystalline structure of SnO_2 nanorods provides additional advantageous features for improving cycling performance and rate capability. First, the presence of thinner subunits (i.e., primary nanorods) as well as their interspaces within the mesocrystalline nanorods may further increase the number of active reaction sites and provide shorter diffusion pathways for lithium ions, thus improving electrocatalytic activity and rate capability [2]. Second, the strong inner connection of the subunits within the mesocrystals may enhance the stability of the bundled primary nanorods, resulting in improved cycling performance. Therefore, the current mesocrystalline SnO_2 nanorod arrays were able to achieve a high initial CE value and retain a high reversible capacity even at a charge/discharge rate as high as 10 C.

4 Conclusions

A general method for facile kinetics-controlled growth of aligned arrays of mesocrystalline SnO_2 nanorods on arbitrary substrates has been developed by carefully adjusting the supersaturation in a unique ternary solvent system comprising acetic acid, ethanol, and water. The hydrolysis processes of Sn(IV) as well as the nucleation and growth of SnO_2 crystals were carefully controlled in the mixed solvents, leading to a heterogeneous nucleation on the substrate and the subsequent growth into mesocrystalline nanorod arrays. The obtained mesocrystalline SnO_2 nanorod arrays grown on Ti foil were used as an anode material for LIBs, which exhibited a superior rate performance with an initial Coulombic efficiency of 65.6% and a reversible capacity of 720 mA·h/g at a current rate of 10 C (namely, 7,820 mA/g). This unusually good rate performance may be attributed to the combination of the 1D nanoarray structure and the unique mesocrystalline structure that improves the electrocatalytic activity and stability. It is expected that the cycling performance and rate capability could be further improved by surface modification or carbon-coating. The anode made of nanorod arrays

on Ti foil has additional advantages such as additive-free electrochemistry and flexible electronics [12]. Furthermore, mesocrystalline SnO_2 nanorod arrays grown on various substrates may find promising applications in some other fields including sensing and photovoltaics. Finally, the kinetics-controlled growth strategy may be extendable to the controlled synthesis of mesocrystalline nanostructure arrays of other functional oxide materials.

Acknowledgements

This work was supported by the National Natural Science Foundation of China (Grant Nos. 21173010, 21073005, and 51121091) and the Ministry of Science and Technology (MOST) of China (Grant No. 2013CB932601).

Electronic Supplementary Material: Supplementary material (further details of the optical photographs, TEM and SEM images, and IR data) is available in the online version of this article at http://dx.doi.org/10.1007/s12274-013-0300-3.

References

[1] Armand, M.; Tarascon, J. M. Building better batteries. *Nature* **2008**, *451*, 652–657.

[2] Song, M. K.; Park, S.; Alamgir, F. M.; Cho, J.; Liu, M. L. Nanostructured electrodes for lithium-ion and lithium-air batteries: The latest developments, challenges, and perspectives. *Mater. Sci. Eng. R* **2011**, *72*, 203–252.

[3] Ji, L. W.; Lin, Z.; Alcoutlabi, M.; Zhang, X. W. Recent developments in nanostructured anode materials for rechargeable lithium-ion batteries. *Energy Environ. Sci.* **2011**, *4*, 2682–2699.

[4] Lee, K. T.; Cho, J. Roles of nanosize in lithium reactive nanomaterials for lithium ion batteries. *Nano Today* **2011**, *6*, 28–41.

[5] Kim, M. G.; Cho, J. Reversible and high-capacity nanostructured electrode materials for Li-ion batteries. *Adv. Funct. Mater.* **2009**, *19*, 1497–1514.

[6] Wang, Y. G.; Li, H. Q.; He, P.; Hosono, E.; Zhou, H. S. Nano active materials for lithium-ion batteries. *Nanoscale* **2010**, *2*, 1294–1305.

[7] Li, H.; Wang, Z. X.; Chen, L. Q.; Huang, X. J. Research on advanced materials for Li-ion batteries. *Adv. Mater.* **2009**, *21*, 4593–4607.

[8] Guo, Y. G.; Hu, J. S.; Wan, L. J. Nanostructured materials for electrochemical energy conversion and storage devices. *Adv. Mater.* **2008**, *20*, 2878–2887.

[9] Bruce, P. G.; Scrosati, B.; Tarascon, J. M. Nanomaterials for rechargeable lithium batteries. *Angew. Chem. Int. Ed.* **2008**, *47*, 2930–2946.

[10] Wang, H. L.; Cui, L. F.; Yang, Y. A.; Casalongue, H. S.; Robinson, J. T.; Liang, Y. Y.; Cui, Y.; Dai, H. J. Mn_3O_4-graphene hybrid as a high-capacity anode material for lithium ion batteries. *J. Am. Chem. Soc.* **2010**, *132*, 13978–13980.

[11] Deng, D.; Kim, M. G.; Lee, J. Y.; Cho, J. Green energy storage materials: Nanostructured TiO_2 and Sn-based anodes for lithium-ion batteries. *Energy Environ. Sci.* **2009**, *2*, 818–837.

[12] Jiang, J. A.; Li, Y. Y.; Liu, J. P.; Huang, X. T. Building one-dimensional oxide nanostructure arrays on conductive metal substrates for lithium-ion battery anodes. *Nanoscale* **2011**, *3*, 45–58.

[13] Wang, Z. Y.; Zhou, L.; Lou, X. W. Metal oxide hollow nanostructures for lithium-ion batteries. *Adv. Mater.* **2012**, *24*, 1903–1911.

[14] Park, M. S.; Wang, G. X.; Kang, Y. M.; Wexler, D.; Dou, S. X.; Liu, H. K. Preparation and electrochemical properites of SnO_2 nanowires for applicaiton in lithium-ion batteries. *Angew. Chem. Int. Ed.* **2007**, *46*, 750–753.

[15] Wang, C.; Zhou, Y.; Ge, M. Y.; Xu, X. B.; Zhang, Z. L.; Jiang, J. Z. Large-scale synthesis of SnO_2 nanosheets with high lithium storage capacity. *J. Am. Chem. Soc.* **2010**, *132*, 46–47.

[16] Huang, J. Y.; Zhong, L.; Wang, C. M.; Sullivan, J. P.; Xu, W.; Zhang, L. Q.; Mao, S. X.; Hudak, N. S.; Liu, X. H.; Subramanian, A. et al., *In situ* observation of the electrochemical lithiation of a single SnO_2 nanowire electrode. *Science* **2010**, *330*, 1515–1520.

[17] Lou, X. W.; Wang, Y.; Yuan, C.; Lee, J. Y.; Archer, L. A. Template-free synthesis of SnO_2 hollow nanostructures with high lithium storage capacity. *Adv. Mater.* **2006**, *18*, 2325–2329.

[18] Wang, Z. Y.; Luan, D. Y.; Boey, F. Y. C.; Lou, X. W. Fast formation of SnO_2 nanobox with enhanced lithium storage capability. *J. Am. Chem. Soc.* **2011**, *133*, 4738–4741.

[19] Wang, Z. Y.; Wang, Z. C.; Madhavi, S.; Lou, X. W. One-step synthesis of SnO_2 and TiO_2 hollow nanostructures with various shapes and their enhanced lithium storage properties. *Chem. Eur. J.* **2012**, *18*, 7561–7567.

[20] Ye, J. F.; Zhang, H. J.; Yang, R.; Li, X. G.; Qi, L. M. Morphology-controlled synthesis of SnO_2 nanosubes by using 1D silica mesostructures as sacrificial templates and their applications in lithium-ion batteries. *Small* **2010**, *6*, 296–306.

[21] Kim, H.; Cho, J. Hard templating synthesis of mesoporous and nanowire SnO_2 lithium battery anode materials. *J. Mater. Chem.* **2008**, *18*, 771–775.

[22] Han, Y. T.; Wu, X.; Ma, Y. L.; Gong, L. H.; Qu, F. Y.; Fan, H. J. Porous SnO_2 nanowire bundles for photocatalyst and Li ion battery applications. *CrystEngComm*, **2011**, *13*, 3506–3510.

[23] Ding, S. J.; Chen, J. S.; Lou, X. W. One-dimensional hierarchical structures composed of novel metal oxide nanosheets on a carbon nanotube backbone and their lithium-storage properties. *Adv. Funct. Mater.* **2011**, *21*, 4120–4125.

[24] Wang, Z. Y.; Zhang, H.; Li, N.; Shi, Z. J.; Gu, Z. N.; Cao, G. P. Laterally confined graphene nanosheets and graphene/SnO_2 composites as high-rate anode materials for lihtium-ion batteries. *Nano Res.* **2010**, *3*, 748–756.

[25] Kim, H.; Kim, S. W.; Park, Y. U.; Gwon, H.; Seo, D. H.; Kim, Y.; Kang, K. SnO_2/graphene composite with high lithium storage capability for lithium rechargeable batteries. *Nano Res.* **2010**, *3*, 813–821.

[26] Ding, S. J.; Luan, D. Y.; Boey, Y. F. C.; Chen, J. S.; Lou, X. W. SnO_2 nanosheets grown on graphene sheets with enhanced lithium storage properties. *Chem. Commun.* **2011**, *47*, 7155–7157.

[27] Ko, Y. D.; Kang, J. G.; Park, J. G.; Lee, S.; Kim, D. W. Self-supported SnO_2 nanowire electrodes for high-power lithium-ion batteries. *Nanotechnology* **2009**, *20*, 455701.

[28] Liu, J. P.; Li, Y. Y.; Huang, X. T.; Ding, R. M.; Hu, Y. Y.; Jiang, J.; Liao, L. Direct growth of SnO_2 nanorod array electrodes for lithium-ion batteries. *J. Mater. Chem.* **2009**, *19*, 1859–1864.

[29] Huang, H.; Lim, C. K.; Tse, M. S.; Guo, J.; Tan, O. K. SnO_2 nanorod arrays: Low temperature growth, surface modification and field emission properties. *Nanoscale* **2012**, *4*, 1491–1496.

[30] Kuang, Q.; Xu, T.; Xie, Z. X.; Lin, S. C.; Huang, R. B.; Zheng, L. S. Versatile fabrication of aligned SnO_2 nanotube arrays by using various ZnO arrays as sacrificial templates. *J. Mater. Chem.* **2009**, *19*, 1019–1023.

[31] Wang, J. Z.; Du, N.; Zhang, H.; Yu, J. X.; Yang, D. R. Large-scale synthesis of SnO_2 nanotube arrays as high-performance anode materials of Li-ion batteries. *J. Phys. Chem. C* **2011**, *115*, 11302–11305.

[32] Vayssieres, L.; Graetzel, M. Highly ordered SnO_2 nanorod arrays from controlled aqueous growth. *Angew. Chem. Int. Ed.* **2004**, *43*, 3666–3670.

[33] Wang, Y. L.; Guo, M.; Zhang, M.; Wang, X. D. Hydrothermal preparation and photoelectrochemical performance of size-controlled SnO_2 nanorod arrays. *CrystEngComm* **2010**, *12*, 4024–4027.

[34] Wang, D. N.; Yang, J. L.; Li, X. F.; Wang, J. J.; Li, R. Y.; Cai, M.; Sham, T. K.; Sun, X. L. Observation of surface/defect states of SnO_2 nanowires on different substrates from X-ray excited optical luminescence. *Cryst. Growth Des.* **2012**, *12*, 397–402.

[35] Cölfen, H.; Antonietti, M. Mesocrystals: Inorganic superstructures made by highly parallel crystallization and controlled alignment. *Angew. Chem. Int. Ed.* **2005**, *44*, 5576–5591.

[36] Song, R. Q.; Cölfen, H. Mesocrystals - ordered nanopartical superstructures. *Adv. Mater.* **2010**, *22*, 1301–1330.

[37] Zhou, L.; O'Brien, P. Mesocrystals-properties and applications. *J. Phys. Chem. Lett.* **2012**, *3*, 620–628.

[38] Cai, J. G.; Ye, J. F.; Chen, S. Y.; Zhao, X. W.; Zhang, D. Y.; Chen, S.; Ma, Y. R.; Jin, S.; Qi, L. M. Self-cleaning, broadband and quasi-omnidirectional antireflective structures based on mesocrystalline rutile TiO_2 nanorod arrays. *Energy Environ. Sci.* **2012**, *5*, 7575–7581.

[39] Ye, J. F.; Liu, W.; Cai, J. G.; Chen, S.; Zhao, X. W.; Zhou, H. H.; Qi, L. M. Nanoporous anatase TiO_2 mesocrystals: Additive-free synthesis, remarkable crystalline-phase stability, and improved lithium insertion behavior. *J. Am. Chem. Soc.* **2011**, *133*, 933–940.

[40] Hong, Z. S.; Wei, M. D.; Lan, T. B.; Jiang, L. L.; Cao, G. Z. Additive-free synthesis of unique TiO_2 mesocrystals with enhanced lithium-ion intercalation properties. *Energy Environ. Sci.* **2012**, *5*, 5408–5413.

[41] Li, W.; Yang, J. P.; Wu, Z. X.; Wang, J. X.; Li, B.; Feng, S. S.; Deng, Y. H.; Zhang, F.; Zhao, D. Y. A versatile kinetics-controlled coating method to construct uniform porous TiO_2 shells for multifunctional core–shell structures. *J. Am. Chem. Soc.* **2012**, *134*, 11864–11867.

[42] Xu, X. X.; Zhuang, J.; Wang, X. SnO_2 quantum dots and quantum wires: Controllable synthesis, self-assembled 2D architectures, and gas-sensing properties. *J. Am. Chem. Soc.* **2008**, *130*, 12527–11535.

[43] Zhang, Z. Y.; Zou, R. J.; Song, G. S.; Yu, L.; Chen, Z. G.; Hu, J. Q. Highly aligned SnO_2 nanorods on graphene sheets for gas sensor. *J. Mater. Chem.* **2011**, *21*, 17360–17365.

[44] Krishnamoorthy, T.; Tang, M. Z.; Verma, A.; Nair, A. S.; Pliszka, D.; Mhaisalkar, S. G.; Ramakrishna, S. A facile route to vertically aligned electrospun SnO_2 nanowires on a transparent conducting oxide substrate for dye-sensitized solar cells. *J. Mater. Chem.* **2012**, *22*, 2166–2172.

[45] Li, H. Q.; Zhou, H. S. Enhancing the performances of Li-ion batteries by carbon-coating: Present and future. *Chem. Commun.* **2012**, *48*, 1201–1217.